Ab initio study of Fermi surface and dynamical properties of Ni_2XAl (X = Ti, V, Zr, Nb, Hf and Ta)

CrossMark

P.V. Sreenivasa Reddy, V. Kanchana *

Department of Physics, Indian Institute of Technology Hyderabad, Ordnance Factory Estate, Yeddumailaram 502 205, Andhra Pradesh, India

ABSTRACT

A detailed study on the pressure and temperature effects on ternary Ni-based inter-metallic compounds Ni_2XAl (X = Ti, V, Zr, Nb, Hf and Ta) have been carried out using density functional theory. The calculated ground state properties are in good agreement with experiments for all the investigated compounds. The band structures and Fermi surface topology is found to be quite similar for all the compounds except for Ni_2NbAl, where we find an extra band to cross the Fermi level under compression resulting in a new electron pocket at X-point. Ni_2NbAl is found to be a superconductor with superconducting transition temperature of 3.1 K which agrees quite well with the experimental value and the calculated T_c is found to vary non-monotonically under pressure. From the calculated phonon dispersion relation, we find all the investigated Ni-based Heusler compounds to be dynamically stable, until high pressure. The ductile nature of these compounds is confirmed from the calculated Cauchy's pressure, Pugh's ratio and Poisson's ratio. In addition, the thermodynamic properties show Ni_2TiAl to have lower specific heat and entropy but higher internal energy and free energy among all the investigated compounds.

© 2014 Elsevier B.V. All rights reserved.

1. Introduction

Ternary intermetallic Heusler alloys Ni_2XAl (X = Ti, Zr, Hf, V, Nb, and Ta) with chemical formula A_2YZ crystallize in cubic $L2_1$-structure, where A and Y are the transition metals and Z is a non-magnetic element [1]. Though the Heusler compounds are well known for their ferromagnetic properties, it is interesting to note the existence of paramagnetic compounds, one among them is the above mentioned series Ni_2XAl [2]. Ni_2TiAl and many other Ni-based compounds have been explored from various perspective, ever since it was found that the high temperature creep resistance of NiAl could be improved by Ti addition [3], which stabilized the compounds in the Heusler type structure. The structural properties of Ni_2TiAl was further studied experimentally by Taylor and Floyd [4], using X-rays and electron spectroscopy and Umakishi et al. [5] further confirmed Ni_2TiAl to have small lattice mismatch with B2 phase and found the same to possess good stability. This series attracted further interest and a complete phase diagram of Ni_2TAl (T = Zr, Nb and Ta) was obtained by Raman and Schubert [6]. Theoretical insight on the above mentioned series was also provided by Lin and Freeman [2] further substantiating the stability of $L2_1$ structure of Ni_2XAl (X = Zr, Nb and Ta). Further, Da Rocha et al.

[7] have reported the specific heat and electronic structure of the above mentioned series. Heusler alloys ever remain a perennial resource of compounds with plethora of studies available explaining the transport, electrical conductivity, magnetic and many other properties owned by them [8–10]. It is further interesting to note that Ni_2NbAl, one among Ni_2XAl being studied, is reported to be a superconductor experimentally with the transition temperature around 2.1 K [11]. Though the binary Ni-based intermetallic compounds were primarily known for high temperature applications [12–16], ternary Ni-intermetallics based on the $L2_1$ structure are found to possess various properties such as superconductivity, magnetism, spintronics [3,17–24], and deserves further investigation which form the main goal of the present work. Our main objective is to explore this series for wide range of applications, for which the electronic structure and the other related properties have to be studied, which is taken up in the present work. Though electronic structures are available for few of these compounds, we focus on the Fermi surface topology, dynamical stability, mechanical and thermodynamics properties of these compounds through computer simulations. In addition, we have also studied the effect of pressure on the Fermi surface and thermodynamic properties, as the Fermi surface topology change can be related to the anomalies observed in the physical properties [25–30]. Recently it was shown that the Fermi surface topology change can be used to predict the trends in the superconducting transition temperature (T_c) [25,26].

* Corresponding author.
E-mail address: kanchana@iith.ac.in (V. Kanchana).

As Ni_2NbAl is a superconductor, we have performed the Fermi surface studies under pressure to predict the trend in the variation of T_c under pressure.

The organization of the paper is as follows. Section 2 given the computational details of the present work. The results and discussions are presented in Section 3 which is again divided into five subsections. Ground state properties and electronic structure properties are given in the first subsection. In this subsection we discuss the band structure, density of states (DOS), Fermi surfaces (FS) of all the compounds at ambient as well as under compression. Elastic constants of all the compounds are calculated using theoretical lattice constant and are discussed in second subsection. Vibrational properties are discussed in third subsection. The superconductivity of Ni_2NbAl is discussed in the fourth subsection. We have discussed the thermodynamic properties in the last subsection. Finally conclusions are presented in Section 4.

2. Methodology

Two distinct density functional calculations have been used in the present work to calculate the electronic structure and vibrational properties. The Full-Potential Linearized Augmented Plane Wave (FP-LAPW) method as implemented in the WIEN2k [31,32] code is used to calculate the electronic structure and Fermi surface properties, and PBE-GGA [33] (Perdew–Burke–Ernzerhof parametrization of the Generalized Gradient Approximation) approximation has been used for the exchange correlation potential. Throughout the calculations, the R_{MT} (radius of muffin tin spheres) value for each atom was fixed as 1.78 a.u. for Ni atom, 1.78 a.u. for X (X = Ti, V, Zr, Nb, Hf and Ta) atom and 1.67 a.u. for Al atom. For the energy convergence, the criterion $R_{MT} * K_{max} = 9$ was used, where K_{max} is the plane wave cut-off. The potential and charge density were Fourier expanded up to $G_{max} = 12$ a.u.$^{-1}$. The valence states included in the calculations are Ni ($3d^8, 4s^2$), Al ($3s^2, 3p^1$), Ti ($3d^2, 4s^2$), V ($3d^3, 4s^2$), Zr ($4d^2, 5s^2$), Nb ($4d^4, 5s^1$), Hf ($4f^{14}, 5d^2, 6s^2$), Ta ($4f^{14}, 5d^3, 6s^2$) and the remaining orbitals are treated as core states. All the electronic properties like band structure, density of states and Fermi surface are calculated with $44 \times 44 \times 44$ k-mesh in the Monkhorst–Pack [34] scheme which gives 2168 k-points in the irreducible part of the Brillouin Zone (BZ) to ensure accurate determination of the Fermi level. For the Brillouin zone integration we have used the tetrahedron method [35]. Birch–Murnaghan [36] equation of state was used to fit the total energies as a function of primitive cell volume to obtain the bulk modulus and the equilibrium lattice parameter for all the investigated compounds.

The thermodynamic properties are calculated using the Quasi-Harmonic Approximation as implemented in the QUANTUM ESPRESSO [37] simulation package with temperature ranging from 0 to 500 K. All the phonon calculations are performed using the plane wave self-consistent field (Pwscf) program based on ultrasoft pseudopotential [38]. These thermodynamic calculations are carried out with the kinetic energy cutoff of 42 Ry (ecutwfc) and the Gaussian broadening of 0.02 Ry (dgauss) and a $4 \times 4 \times 4$ uniform grid of q-points are used for all the compounds. The

exchange–correlation functional of PBE within the GGA is used for the calculations. We have calculated the electron–phonon coupling constant λ_{ep} by using Eliashberg function for Ni_2NbAl and with this λ_{ep} the T_c is calculated using the Allen–Dynes formula [39]. The temperature dependent bulk modulus and linear expansion coefficient for all the compounds are also calculated using GIBBS2 program [40].

3. Results and discussion

3.1. Ground state and electronic structure (band structure, density of states and Fermi surface) properties

The basic ground state properties are calculated using the Birch–Murnaghan equation of state and the results are reported in 1, along with the available experimental results. From the calculated values, we see that the maximum error in the lattice parameter is 0.47% for Ni_2TiAl and the minimum error is 0.03% for Ni_2VAl.

Electronic structure of all the investigated compounds are studied at ambient as well as under compression. The semi-relativistic band structure of these compounds are shown in Fig. 1. We have also checked the effect of Hubbard 'U' and found no appreciable changes in the band structure as these are metallic systems and are not correlated. This is consistent with the recent studies on Heusler based compounds where the authors also concluded the same [41]. The overall profile of all these Ni_2XAl compounds are the same, whereas the number of bands crossing the E_F is not the same for all the compounds. For Ni_2TiAl, Ni_2ZrAl and Ni_2HfAl three bands cross the E_F, two of them crossing at the L-point from valence band to conduction band (Here the conduction bands refer to the bands above the Fermi level and they are primarily X-derived states) and the third band crosses the E_F from conduction band to valence band at X-point (band structure of Ni_2TiAl is shown in Fig. 1). For Ni_2VAl, we observe two bands to cross the Fermi level at X-point from conduction band to valence band. For Ni_2NbAl and Ni_2TaAl compounds, we find only one band to cross the E_F from conduction band to valence band at X-point at ambient condition.

To analyze in detail, we have also calculated the density of states for all these compounds as shown in Fig. 2 and it is evident that the contribution at E_F is mainly dominated by Ni-d_{e_g} states with an admixture of X-$d_{t_{2g}}$ and Al-p states. The states at nearly -6 eV is mainly derived from the Al-s states. For all the compounds the bonding and the anti-bonding regions are well separated from the non-bonding region and our calculations agree well with the earlier studies [2]. As we move to compounds containing V-B elements we could see the states to shift below E_F due to band filling and is clearly evident from Fig. 2. Apart from this, our calculated density of states at the Fermi level show a decreasing trend as we move from top to bottom of the periodic table.

In addition, the Fermi surfaces of all the investigated compounds at ambient conditions are shown in Fig. 3, for the corresponding band which crosses the E_F as shown in Fig. 1. We observe the Fermi surface topology to be quite similar for Ni_2TiAl, Ni_2ZrAl and Ni_2HfAl (FS for Ni_2ZrAl and Ni_2HfAl compounds are not

Table 1
The calculated theoretical lattice parameter (a_{the}) compared with the experimental lattice parameter (a_{exp}), bulk modulus (B), density of states at the Fermi level ($N(E_F)$) (states/eV/f.u.) and Somerfield coefficient (γ) (mJ/mol K^2) of Ni_2XAl (X = Ti, Zr, Hf, V, Nb, Ta).

Parameters	Ti	Zr	Hf	V	Nb	Ta
a_{the} (Å)	5.90	6.13	6.10	5.80	5.99	5.98
a_{exp} (Å)	5.87 [2]	6.12 [2]	6.08 [2]	5.80 [7]	5.97 [2]	5.96 [7]
B (GPa)	164	151	158	181	181	191
DOS $N(E_F)$	3.50	3.25	2.81	3.51	2.27	2.13
γ	8.25	7.65	6.63	8.27	5.36	5.02
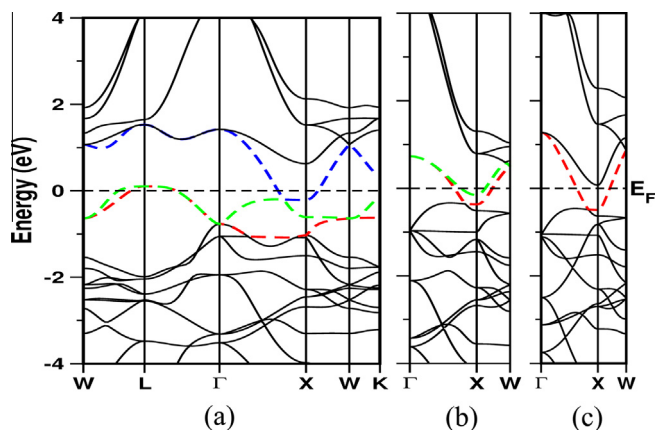
Fig. 1. Band structure at ambient condition (at experimental volume) for (a) Ni$_2$TiAl (same for Ni$_2$ZrAl and Ni$_2$HfAl), (b) Ni$_2$VAl and (c) Ni$_2$NbAl (same for Ni$_2$TaAl).

displayed) indicating the dominating nature of the Ni-d states with small contribution from X-d states at E_F. For Ni$_2$TiAl, Ni$_2$ZrAl and Ni$_2$HfAl compounds which contain IV-B elements we find the Fermi surface to be of electron character at X-point and hole character at L-point respectively and is also evident from the band structure plot from Fig. 1, whereas in Ni$_2$VAl, Ni$_2$NbAl and Ni$_2$TaAl compounds which contain V-B elements, we find the band to cross only at X-point resulting in the electron pocket at the same point. From Fig. 3(d) and (e) it is evident that Ni$_2$VAl has two FS as a result of two bands crossing the E_F (see Fig. 1(b)) and the remaining two compounds Ni$_2$NbAl, Ni$_2$TaAl have only one FS, due to a single band crossing the E_F (see Fig. 1(c)).

We have also studied the band structure and Fermi surface under compression. For all these compounds under study, we observe the FS topology to remain unaltered under compression with slight change in the size of the electron or hole pocket, which might be due to the bands crossing the Fermi level being less dispersive at the high symmetry points. Under compression an interesting feature to note is that, we find an additional electron pocket to appear in Ni$_2$NbAl at around $V/V_0 = 0.93$ (pressure of 17 GPa) which is due to the band dropping down the E_F at the X-point and is shown in Fig. 4(a) and the corresponding Fermi surfaces are shown in Fig. 4(b) and (c).

3.2. Elastic constants

To account for the mechanical stability of all the investigated compounds we have calculated the elastic constants. All the above mentioned compounds crystallize in the cubic structure and have three non-zero elastic constants C_{11}, C_{12}, C_{44}. The calculated single crystal elastic constants at equilibrium volume are given in Table 2 for all the compounds. The calculated elastic constants of all the compounds satisfy the Born mechanical stability criteria [42] i.e. $C_{11} > 0$, $C_{44} > 0$, $C_{11} > C_{12}$, and $C_{11} + 2C_{12} > 0$, which indicate these compounds to be mechanically stable at ambient condition. From the single crystal elastic constants, we have calculated the Young's modulus E, Voigt–Reuss–Hill modulus G_H [43], Poisson's ratio σ, Anisotropy factor A and are reported in Table 2. The relations between C_{11}, C_{12}, C_{44} and the above mentioned parameters can be found elsewhere [44–47].

Debye temperature (Θ_D) is one of the most important parameter and it determines the thermal characteristics of the materials. The Debye temperature can be obtained from the mean sound
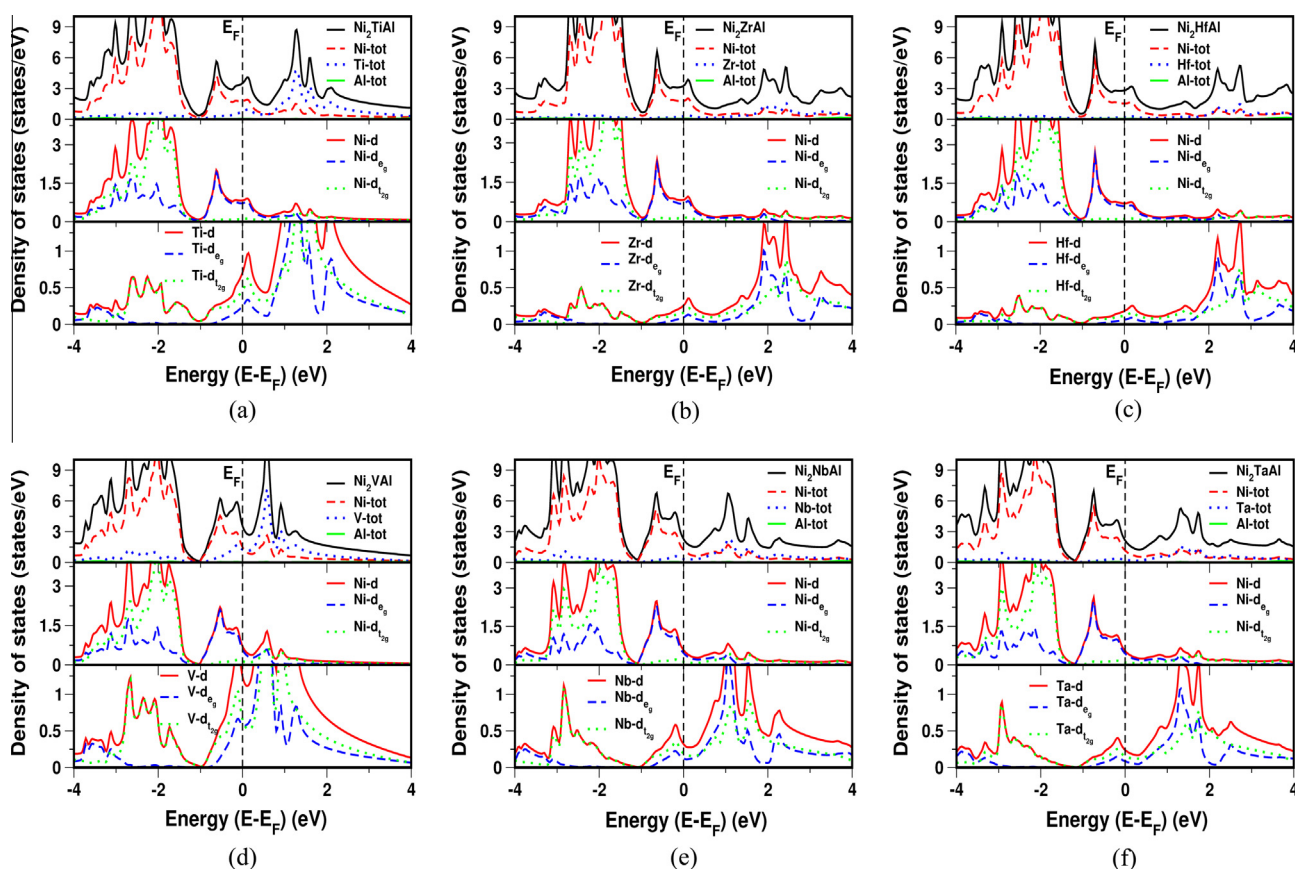
Fig. 2. Density of states at ambient (at experimental volume) for (a) Ni$_2$TiAl, (b) Ni$_2$ZrAl, (c) Ni$_2$HfAl, (d) Ni$_2$VAl, (e) Ni$_2$NbAl and (f) Ni$_2$TaAl compounds.
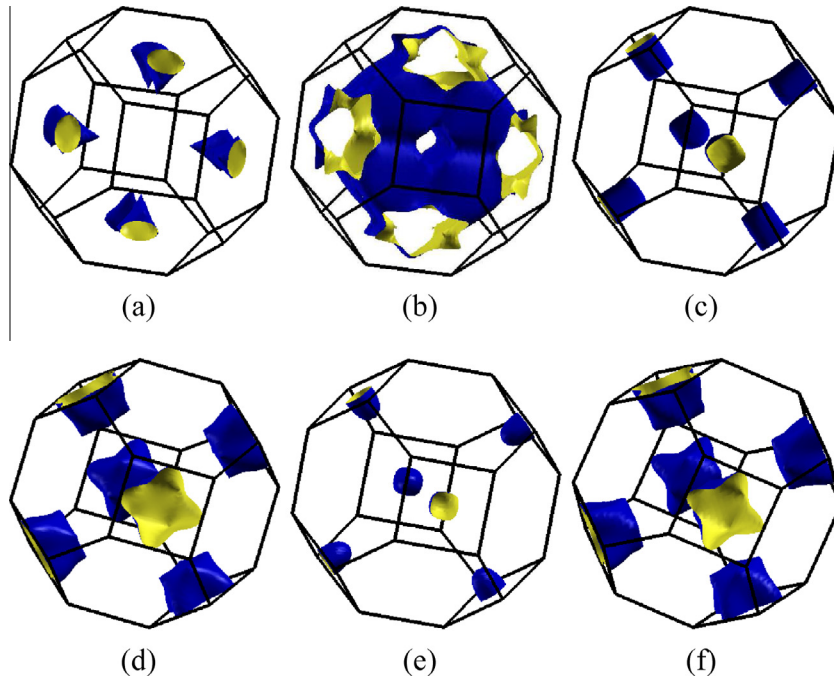
Fig. 3. Fermi surfaces of (a–c) Ni$_2$TiAl (same for Ni$_2$ZrAl and Ni$_2$HfAl), and (d and e) Ni$_2$VAl, (f) Ni$_2$NbAl (same for Ni$_2$TaAl) at experimental volume.
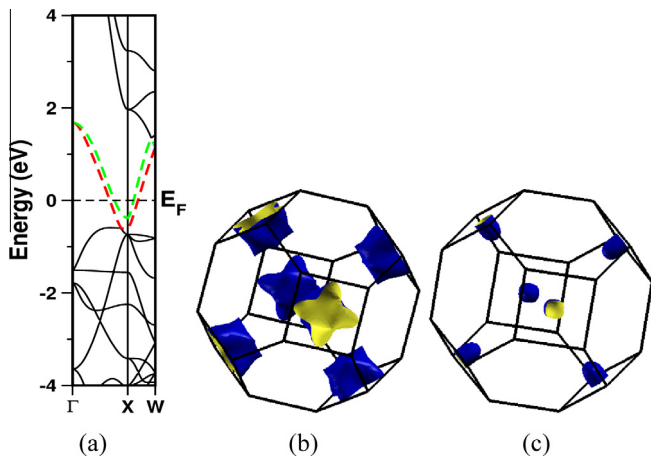
Fig. 4. (a) Band structure under compression (at $V/V_0 = 0.93$, where V_0 is the experimental volume) for Ni$_2$NbAl compound and the corresponding FS and (b and c) at the same compression.

velocity, which gives the explicit information about lattice vibration and can be computed directly from the given relation.

$$\Theta_D = \frac{h}{k}\left[\frac{3n}{4\pi}\left(\frac{\rho N_A}{M}\right)\right]^{1/3} v_m \tag{1}$$

where 'h' is the Planck's constant, 'k' is the Boltzmann's constant, 'N_A' is the Avogadro's number, 'ρ' is the density, 'M' is the molecular weight, 'n' is the number of atoms in the unit cell, and 'v_m' is the mean sound velocity, which can be calculated by using the following relation.

$$v_m = \left[\frac{1}{3}\left(\frac{2}{v_t^3} + \frac{1}{v_l^3}\right)\right]^{-1/3} \tag{2}$$

where 'v_l' and 'v_t' are the longitudinal and transverse sound velocities obtained using the shear modulus G_H and the bulk modulus B.

$$v_l = \sqrt{\frac{(B + \frac{4}{3}G_H)}{\rho}} \tag{3}$$

$$v_t = \sqrt{\frac{G_H}{\rho}} \tag{4}$$

The calculated values for all the above defined parameters are given in Table 2. From Table 2, it is seen that Ni$_2$TiAl has higher Young's modulus in comparison with other compounds which might imply Ni$_2$TiAl to be stiffer among the other compounds studied. The elastic anisotropy gives the possibility of inducing micro cracks in the materials [44] and the calculated value of the elastic anisotropy of all the studied compounds are given in Table 2.

The Cauchy's pressure ($C_{12} - C_{44}$) can be used to comment on the ductile or brittle nature of the compounds. Here Cauchys pressure for all the compounds is positive indicating the ductile nature. Pugh's ratio ($\frac{G_H}{B}$) [48] is another index for explaining the ductile and brittle nature of the compounds. Larger and smaller values of Pugh's ratio indicate the brittle and ductile nature of the material respectively. The critical number which separates the ductile and brittle nature was reported to be 0.57. This series of compounds have the Pugh's ratio values lesser than this critical number indicating the ductile nature. The Poisson's [49] ratio indicate the stability of the crystal against shear and takes the values in between −1 to 0.5, where −1 and 0.5 serve as lower and upper bounds respectively. The lower bound is the one where the materials does not change its shape and the upper bound is where the volume remains unchanged. These compounds have the Poisson's ratio values closer to the upper limit indicating the stiffness of these compounds. From the reported values as shown in Table 2, we could see the Poisson's ratio to be higher for the compounds having IV-B group elements and lower for compounds which have V-B group elements. The Debye temperature which is used to estimate the thermal properties of material is also calculated with the help of mean sound velocity. From Table 2, we find Debye temperature and mean sound velocities to decrease as we move from top to bottom in the periodic table and higher θ_D values indicate higher thermal conductivity associated with these compounds.

3.3. Vibrational properties

We have also calculated the phonon dispersion along the high symmetry directions of the Brillouin zone to find the dynamical stability of these compounds at ambient as well as under compression along with the phonon density of states and are shown in Fig. 5. The unit cell of Ni$_2$XAl contains four atoms, which gives rise to 12 phonon branches in all, out of which three are acoustical and nine are optical modes. However this number is reduced in different directions due to degeneracy. The absence of imaginary frequency in all high symmetry direction for all the investigated compounds confirm the dynamical stability at ambient as well as under compression. The same stability was not found for other Ni-based Heusler alloys, Ni$_2$MnAl and Ni$_2$MnGa reported earlier due to the presence of the imaginary frequencies [50,22]. We find all the phonon modes to harden under compression as evident from Fig. 6 and is further confirmed from the mode Grüneisen parameters as reported in 3, which is a most important physical quantity, relating the volume variation with the phonon frequencies and is defined as

$$\gamma_i = \partial(ln\omega_i)/\partial(lnV) \tag{5}$$

where ω_i is the frequency of the specific mode and V is the volume. These values again confirm the dynamical stability of these studied compounds until high pressure, which is seen from the obtained positive slope for all the modes. Again the hardening of phonon modes are more pronounced for the compounds which have V-B group elements than the compounds having IV-B group elements. We observed that for all the compounds maximum contribution at higher and lower frequency regions is mainly from Al, Ni atoms respectively. In the middle frequency region for Ni$_2$XAl (X = Ti, V, Zr, Nb) compounds the maximum contribution is from X atom and in the case of Ni$_2$HfAl and Ni$_2$TaAl, Ni atoms are found to contribute more in the same region. The vibrational properties and mode Grüneisen parameter confirm the stability of these compounds till high pressure and we proceed further to analyze the superconductivity of Ni$_2$NbAl.

3.4. Superconductivity of Ni$_2$NbAl

It is well known from the earlier studies that the FS topology change under pressure can be related to many other changes in the physical properties of the compounds [25–30]. Among all the above mentioned compounds Ni$_2$NbAl is reported to be a superconductor, with a superconducting transition temperature (T_c) to be around 2.1 K. We have also calculated T_c for Ni$_2$NbAl and found the value to be around 3.1 K with electron-phonon coupling

constant (λ_{ep}) to be 0.76 and ω_{ln} (logarithmically averaged phonon frequency) to be 70.94 cm^{-1} using Allen–Dynes [39] formula as given in Eq. (6) by considering the value of μ^* (Coulomb pseudopotential), to be 0.15. Our calculated value of λ_{ep} slightly overestimate the earlier reported experimental value of 0.52 [11].

$$T_c = \frac{\omega_{ln}}{1.2} exp\left(-\frac{1.04(1 + \lambda_{ep})}{\lambda_{ep} - \mu^*(1 + 0.62\lambda_{ep})}\right) \tag{6}$$

and

$$\lambda_{ep} = \frac{N(\epsilon_f)\langle I^2 \rangle}{M\langle \omega^2 \rangle} \tag{7}$$

where $N(\epsilon_f)$ = electron density of states, $\langle I^2 \rangle$ = mean square of electron-ion interaction, M = atomic mass and $\langle \omega^2 \rangle$ = average of square of phonon frequency.

As stated above, under compression, we find a new electron pocket to appear in Ni$_2$NbAl at around $V/V_0 = 0.93$, which enable us to throw light on the prediction of T_c under pressure. From our earlier work on superconductors [25,26], we could expect a non-monotonic variation of density of states in the compounds, where we observe a FS topology change, which prompt us to search for the same in the present compound also and the density of states variation as a function of relative volume is shown in Fig. 6(a) which presents a non-monotonic trend. Apart from this we have also plotted the Eliashberg function ($\alpha^2F(\omega)$) in Fig. 6(b), where we find the Eliashberg function to be highest in the lower frequency region indicating Ni atom to contribute more for T_c as evident from the partial phonon density of states from Fig. 5(e). In addition we have also calculated the T_c under compression and find T_c to decrease initially, followed by an increase in accordance with the electron phonon coupling constant as shown in Fig. 7. Apart from this we have also plotted the variation of ω_{ln} as a function of pressure and find ω_{ln} to increase initially and then to decrease under pressure which according to the formula (7), implies an inverse proportionality with λ_{ep} and it is shown in Fig. 7. Further, the variation of T_c under pressure, almost follows the same trend as that of λ_{ep}, which might enable us to predict that phonon contribution may be dominant in this compound.

3.5. Thermodynamic properties

To investigate the thermodynamic properties of Ni$_2$XAl, we have used quasi-harmonic approximation as implemented in Quantum Espresso [37]. In this approximation Helmholtz free energy at a given volume V and temperature T is given as

$$F(V,T) = U_0(V) + F_{vib}(V,T) \tag{8}$$

where U_0 is the the energy corresponding to zero temperature, and F_{vib} represents the vibrational contribution and it can be written as

$$F_{vib}(V,T) = \frac{1}{2}\sum_{n,q}\hbar w(n,q) + K_BT\sum_{n,q}\ln(1 - e^{-\hbar w(n,q)/K_BT}) \tag{9}$$

The frequency of the nth mode, $w(n,q)$, depends on the unit cell volume and the masses of the constituent atoms. The calculated thermodynamic properties like specific heat at constant volume (C_V), entropy (S) and internal energy (U) are shown in Figs. 8 and 9.

The temperature dependence of internal energy, vibrational free energy, entropy and heat capacity at constant volume are shown in Fig. 8 at ambient with temperature ranging from 0 K to 500 K. We have observed that the temperature variation of these thermodynamic functions exhibit almost a similar trend for all investigated compounds. The results of the internal energy from Fig. 8(a) suggest that, above 200 K, the total internal energies increase almost linearly with temperature for all the compounds. At high temperatures the internal energy tends to display k_BT

Table 2
Calculated elastic constants and derived quantities for Ni$_2$XAl (X = Ti, Zr, Hf, V, Nb, Ta) at the theoretical lattice constant. v_l, v_t, v_m are the longitudinal, transverse and mean sound velocities. (CP = Cauchy's pressure).

Parameters	Ti	Zr	Hf	V	Nb	Ta
C_{11} (GPa)	223	217	211	200	212	229
C_{12} (GPa)	135	119	132	171	167	172
C_{44} (GPa)	104	81	90	109	98	109
E (GPa)	193	174	171	138	150	172
A	2.36	1.65	2.27	7.69	4.37	3.89
CP	30.18	37.41	41.64	62.33	68.26	63.01
Pugh's ratio	0.45	0.44	0.41	0.28	0.30	0.33
σ	0.30	0.31	0.32	0.37	0.36	0.35
G_H (GPa)	74.00	66.37	64.85	50.43	54.99	63.79
v_l (km/s)	13.00	11.88	10.17	12.22	11.81	10.48
v_t (km/s)	6.89	6.25	5.24	5.51	5.48	5.04
v_m (km/s)	7.71	6.99	5.86	6.21	6.17	5.66
Θ_D (K)	617.89	539.17	454.73	506.42	487.11	446.99
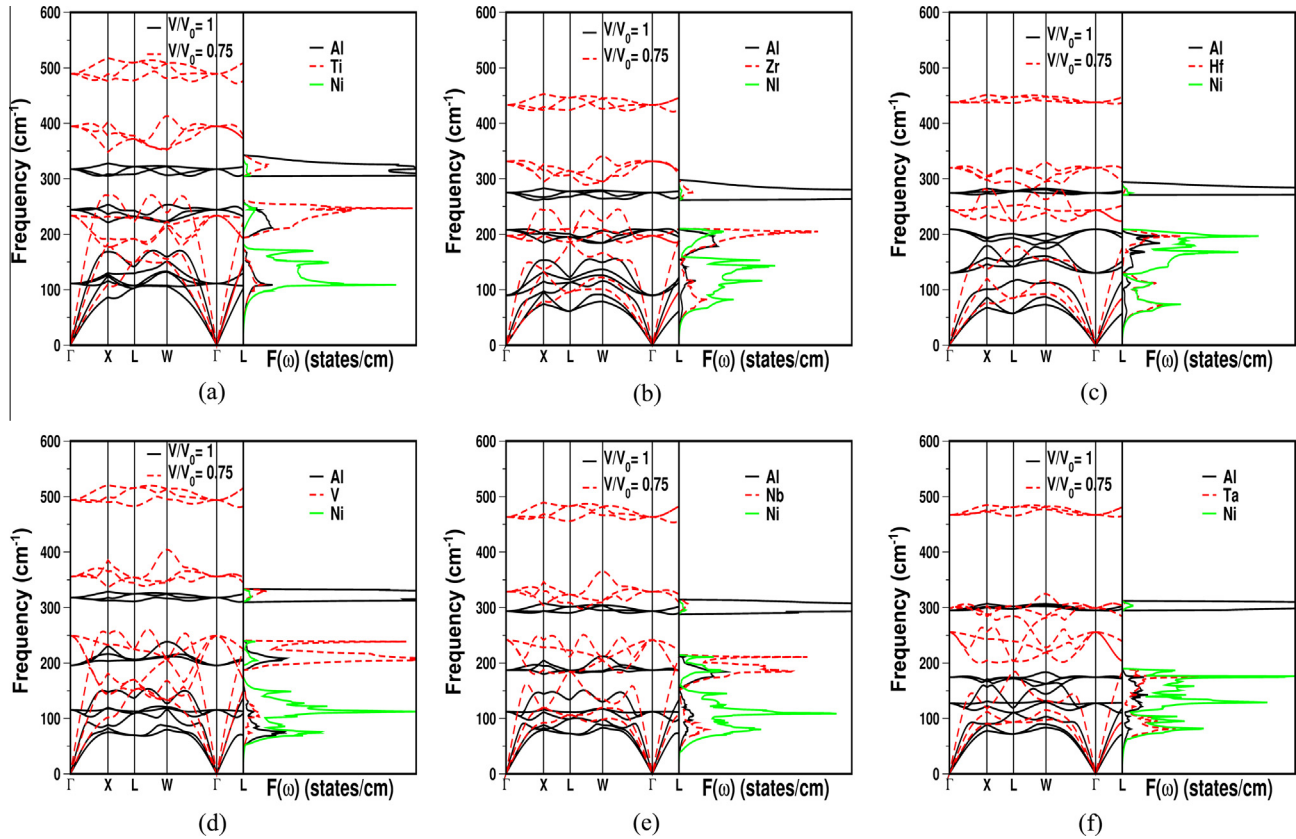
Fig. 5. Phonon dispersion at ambient (solid line) and under compression (at $V/V_0 = 0.75$, where V_0 is the experimental volume) (dotted line) along with phonon density of states ($F(\omega)$) (at ambient) for (a) Ni$_2$TiAl, (b) Ni$_2$ZrAl, (c) Ni$_2$HfAl, (d) Ni$_2$VAl, (e) Ni$_2$NbAl and (f) Ni$_2$TaAl.
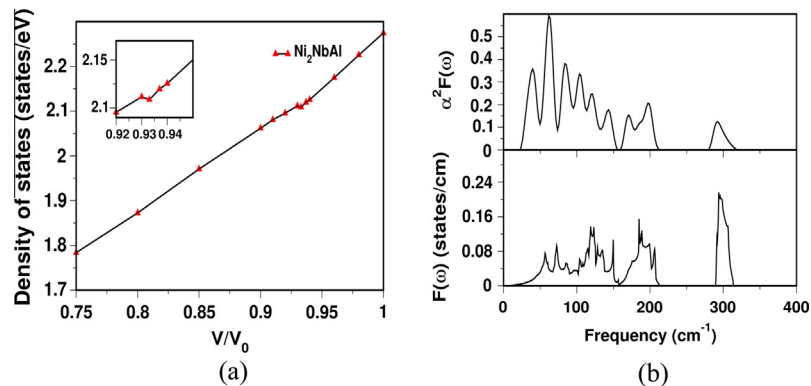
Fig. 6. (a) Density of states at the Fermi level $N(E_F)$ under compression and (b) Eliasberg function $\alpha^2 F(\omega)$ and phonon-density of states for Ni$_2$NbAl compound.

Table 3
Grüneisen mode parameter at Gamma point for Ni$_2$XAl (X = Ti, Zr, Hf, V, Nb, Ta).

Mode	Ti	Zr	Hf	V	Nb	Ta
T_{2g}	2.16	2.22	2.02	2.14	2.55	2.41
T_{1u}	1.48	1.46	1.41	2.08	1.97	1.74
T_{1u}	1.43	1.46	1.55	2.08	1.59	1.62

behavior. Fig. 8(b) shows the variation of vibrational free energy as a function of temperature for the same compounds. Overall, free energy profiles of all the studied compounds show similar characteristics and the free energy $F = U - TS$, where U is internal energy and S is entropy, decreases gradually with increasing temperature. This is because of the fact that both U and S increases with

temperature which lead to the decrease in free energy [51]. The free energy and internal energy at zero Kelvin temperature represent the zero point motion of the compounds. The calculated values of the free and internal energies for the compounds are close to each other and Ni$_2$TiAl have the highest value and Ni$_2$ZrAl have the lowest values at zero point temperature. The free energy calculations indicate that Ni$_2$TiAl is thermodynamically stable. The variation of entropy with temperature for all these compounds in the same temperature range is given in Fig. 8(c). From this figure we have observed that at 0 K the entropies are zero for all compounds and the entropy change increase rapidly as temperature increases. At above 350 K the variation of entropy is small. This change in entropy is due to the increase of the vibrational motion of the atoms with temperature leading to the increase in the internal energy of the system. From this figure we observe that Ni$_2$TiAl have
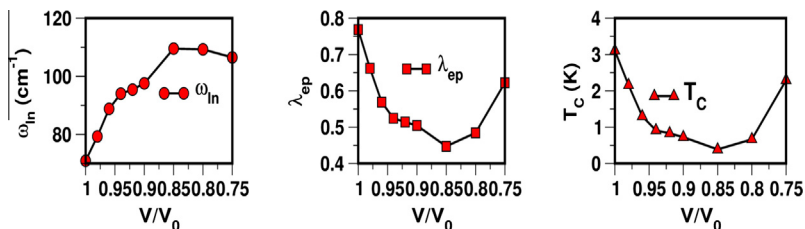
Fig. 7. Logarithmically averaged phonon frequency (ω_{ln}), electron–phonon coupling constant (λ_{ep}) and transition temperature (T_c) for Ni₂NbAl compound under compression.
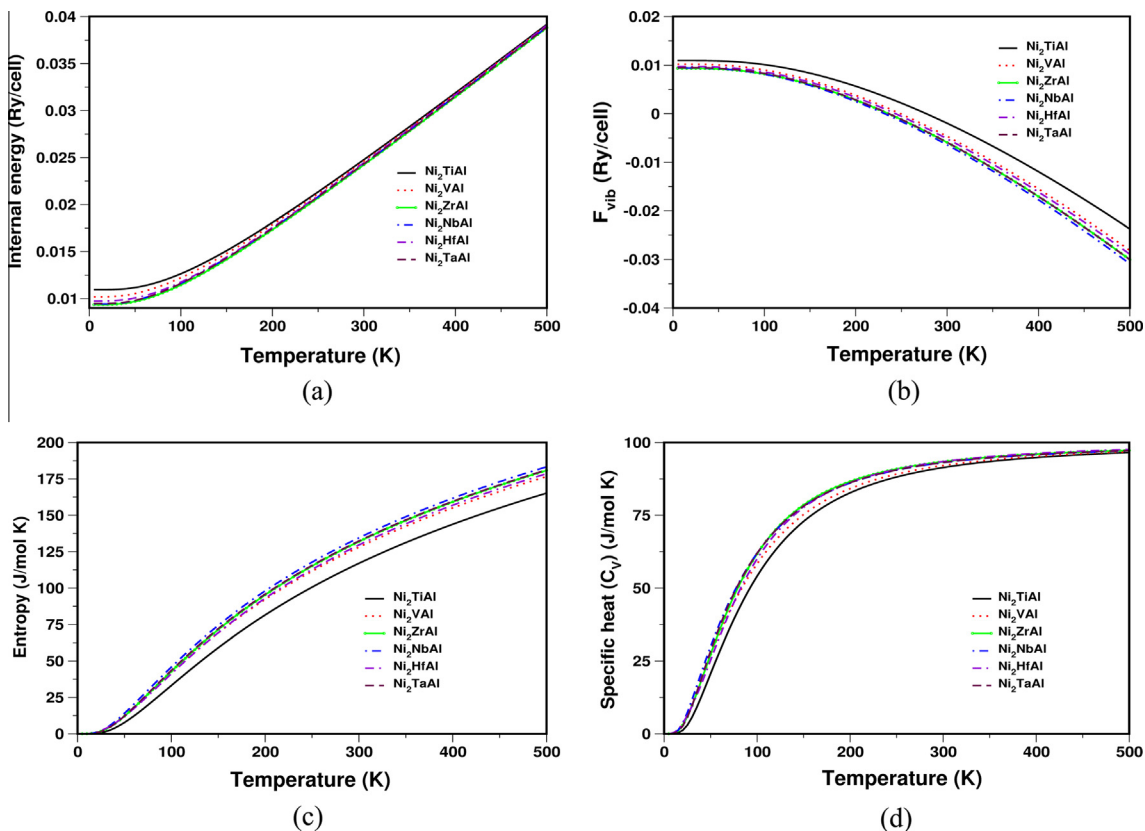
Fig. 8. Variation of thermodynamic properties with temperature at ambient (at $V/V_0 = 1.00$, where V_0 is the experimental volume) (a) internal energy, (b) vibrational free energy, (c) entropy and (d) specific heat.
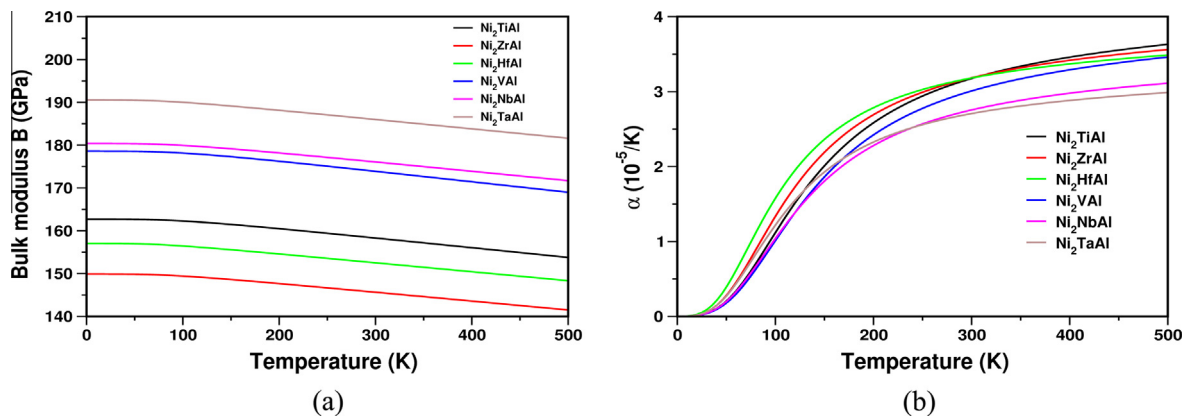
Fig. 9. (a) Variation of bulk modulus with temperature and (b) linear thermal expansion coefficient Ni₂XAl (X = Ti, Zr, Hf, V, Nb, Ta) as a function of temperature.

the minimum entropy values, which indicate Ni₂TiAl to be highly ordered in comparison with other compounds. The specific heat capacity is a measure of how well the substance stores the heat.

The calculated specific heat as a function of temperature for all the investigated compounds are shown in Fig. 8(d). From this we can clearly see that at high temperatures the specific heat at

constant volume obeys Dulong Petit limit, and at low temperatures it is proportional to T^3 law. At the intermediate temperatures, the temperature dependence of specific heat is governed by the details of vibrations of the atoms. From this figure we have observed that Ni_2TiAl has the lowest value of specific heat compared to other compounds.

To explore further we have also calculated the bulk modulus (B), which measures the resistance of the substance to uniform compression and linear thermal expansion (α) as a function of temperature. The calculated temperature variation of bulk modulus (B) is given in Fig. 9(a). From the figure we can see the bulk modulus to decrease with increase in temperature for all the compounds studied. The calculated values of linear thermal expansion coefficient (α) as a function of temperature is shown in Fig. 9(b). From this figure, we observe that all the compounds show positive thermal expansion coefficient and at high temperatures, the compounds containing IV-B group elements possess higher α values than the compounds containing V-B group elements. Among all the compounds at high temperatures Ni_2TiAl has the highest α value whereas Ni_2TaAl is found to have the lowest α value.

4. Conclusions

We have studied the electronic, mechanical, vibrational, thermodynamical and Fermi surface properties of all the investigated compounds using first principles calculations. The obtained structural parameters are in good agreement with the experimental and other theoretical data at ambient condition. Under compression we find an extra band to cross the E_F in the case of Ni_2NbAl resulting in a new electron pocket at X-point. Ni_2NbAl is found to be a superconductor with T_c around 3.1 K in good agreement with experiment. A non-monotonic variation in the DOS is observed in Ni_2NbAl, which may further indicate a non-monotonic variation of T_c under pressure, which is also observed from the present calculations. From elastic constants and the related mechanical properties, we find all the compounds to be ductile in nature with elastic anisotropy. Apart from this, the mechanical and the dynamical stability of these compounds are verified from our calculated elastic constants and the phonon dispersion relation, respectively. The phonon hardening observed in all the compounds under compression is also confirmed from the calculated mode Grüneisen parameter. Among all the investigated compounds, Ni_2TiAl has the lowest specific heat and entropy, and highest internal energy, vibrational free energy and linear thermal expansion coefficient, which might enable Ni_2TiAl to find promising applications.

Acknowledgments

References

[1] T. Graf, C. Felser, S.S.P. Parkin, Prog. Solid State Chem. 39 (2011) 1.
[2] W. Lin, A.J. Freeman, Phys. Rev. B 45 (1992) 61.
[3] P.R. Strutt, R.S. Polvani, J.C. Ingram, Metall. Mater. Trans. A 7A (1976) 23.
[4] A. Taylor, R.W. Floyd, J. Inst. Met. 81 (1952) 25.
[5] Y. Umakishi, M. Yamaguchi, T. Yamane, Philos. Mag. A 52 (1985) 357.
[6] A. Raman, K. Schubert, Z. Metallik. 56 (1965) 99.
[7] F.S. Da Rocha, G.L.F. Fraga, D.E. Brandao, C.M. Da Silva, A.A. Gomes, Physica B 269 (1999) 154.
[8] J. Sahariya, B.L. Ahuja, Physica B 407 (2012) 4182.
[9] E. Shreder, S.V. Streltsov, A. Svyazhin, A. Makhnev, V.V. Marchenkov, A. Lukoyanov, H.W. Weber, J. Phys.: Condens. Matter 20 (2008) 045212.
[10] Y. Miura, M. Shirai, K. Nagao, J. Appl. Phys. 99 (2006). 08J112.
[11] S. Waki, Y. Yamaguchi, K. Mitsugi, J. Phys. Soc. Jpn. 54 (1985) 1673.
[12] R. Darolia, J. Miner., Met. Mater. Soc. 43 (1991) 44.
[13] A.I. Taub, Fleischer, Science 243 (1989) 616.
[14] R.L. Fleischer, Platinum Met. Rev. 36 (1992) 138.
[15] M. Yamaguchi, H. Inui, K. Ito, Acta Mater. 48 (2000) 307.
[16] D.G. Morris, M.A. Muñoz-Morris, Rev. Met. Madrid Extr. (2005) 498.
[17] J. Winterlik, G.H. Fecher, A. Thomas, C. Felser, Phys. Rev. B 79 (2009) 064508.
[18] K. Ramesh Kumar, V. Chunchu, A. Thamizhavel, J. Appl. Phys. 113 (2013) 17E155.
[19] T. Klimczuk, C.H. Wang, K. Gofryk, F. Ronning, J. Winterlik, G.H. Fecher, J.-C. Griveau, E. Colineau, C. Felser, J.D. Thompson, D.J. Safarik, R.J. Cava, Phys. Rev. B 85 (2012) 174505.
[20] W. Ming, Y. Liu, W. Zhang, J. Zhao, Y. Yao, J. Phys.: Condens. Matter 21 (2009) 075501.
[21] S. Picozzi, A. Continenza, A.J. Freeman, J. Phys. D: Appl. Phys. 39 (2006) 851.
[22] A.T. Zayak, P. Entel, K.M. Rabe, W.A. Adeagbo, M. Acet, Phys. Rev. B 72 (2005) 054113.
[23] G.T. De Laissardiere, D.N. Manh, L. Magaud, J.P. Julien, F. Cyrot-Lackmann, D. Mayou, Phys. Rev. B 52 (1995) 7920.
[24] H. Fu, D. Chen, X. Chenga, T. Gao, X. Yang, Physica B 388 (2007) 303.
[25] S. Ram, V. Kanchana, G. Vaitheeswaran, A. Svane, S.B. Dugdale, N.E. Christensen, Phys. Rev. B 85 (2012) 174531.
[26] S. Ram, V. Kanchana, A. Svane, S.B. Dugdale, N.E. Christensen, J. Phys.: Condens. Matter 25 (2013) 155501.
[27] S. Huang, C.W. Chu, F.Y. Fradin, L.B. Welsh, Solid State Commun. 16 (1975) 409.
[28] A. Landa, J. Klepeis, P. Soderlind, I. Naumov, O. Velikokhatnyi, L. Vitos, A. Ruban, J. Phys.: Condens. Matter 18 (2006) 5079.
[29] H. Rosner, D. Koudela, U. Schwarz, A. Handstein, M. Hanfland, I. Opahle, K. Koepernik, M.D. Kuzmin, K.H. Muller, J.A. Mydosh, M. Richter, Nat. Phys. 2 (2006) 469.
[30] D. Koudela, M. Richter, A. Möbius, K. Koepernik, H. Eschrig, Phys. Rev. B 74 (2006) 214103.
[31] P. Blaha, K. Scwarz, P. Sorantin, S.B. Tricky, Comput. Phys. Commun. 59 (1990) 399.
[32] P. Blaha, K. Scwarz, G.K.H. Madsen, D. Kvasnicka, J. Luitz, in: K. Schwarz (Ed.), WIEN2k, An Augumented Plane Wave Plus Local Orbital Programe for Calculating Crystal Properties. Austria: Tech. Techn. Universität wien, Austria, 2001 (ISBN 3-9501031-1-2).
[33] J.P. Perdew, K. Burke, M. Ernzerhof, Phys. Rev. Lett. 77 (1996) 3865.
[34] H.J. Monkhorst, J.D. Pack, Phys. Rev. B 13 (1976) 5188.
[35] P.E. Blochi, O. Jepsen, O.K. Andersen, Phys. Rev. B 49 (1994) 16223.
[36] F. Birch, Phys. Rev. 71 (1947) 809.
[37] P. Giannozzi, S. Baroni, N. Bonini, M. Calandra, R. Car, C. Cavazzoni, D. Ceresoli, G.L. Chiarotti, M. Cococcioni, I. Dabo, A.D. Corso, S. de Gironcoli, S. Fabris, G. Fratesi, R. Gebauer, U. Gerstmann, C. Gougoussis, A. Kokalj, M. Lazzeri, L. Martin-Samos, N. Marzari, F. Mauri, R. Mazzarello, S. Paolini, A. Pasquarello, L. Paulatto, C. Sbraccia, S. Scandolo, G. Sclauzero, A.P. Seitsonen, A. Smogunov, P. Umari, R.M. Wentzcovitch, J. Phys.: Condens. Matter 21 (2009) 395502.
[38] S. Baroni, S.D. Gironcoli, A. dal Corso et al., 2008 <http://www.pwscf.org>.
[39] P.B. Allen, R.C. Dynes, J. Phys. C: Solid State Phys. 8 (1987) L158.
[40] A. Otero-de-la-Roza, V. Luaña, Comput. Phys. Commun. 182 (2011) 1708.
[41] E. Şaşioğlu, I. Galanakis, C. Friedrich, S. Blügel, Phys. Rev. B 88 (2013) 134402.
[42] M. Born, J. Chem. Phys. 7 (1939) 591.
[43] R. Hill, Proc. Phys. Soc. A 65 (1952) 349.
[44] V. Kanchana, Eur. Phys. Lett. 87 (2009) 26006.
[45] V. Kanchana, G. Vaitheeswaran, Ma Yanming, Yu Xie, A. Svane, O. Eriksson, Phys. Rev. B 80 (2009) 125108.
[46] V. Kanchana, G. Vaitheeswaran, A. Svane, A. Delin, J. Phys.: Condens. Matter 18 (2006) 9615.
[47] V. Kanchana, G. Vaitheeswaran, A. Svane, J. Alloy Comp. 455 (2008) 480.
[48] S.F. Pugh, Philos. Mag. 45 (1954) 823.
[49] J.J. Wortman, R.A. Evans, J. Appl. Phys. 36 (1965) 153.
[50] C. Bungaro, K.M. Rabe, A. Dal Corso, Phys. Rev. B 68 (2003) 134104.
[51] K. Ramesh Babu, Ch. Bheema Lingam, S. Auluck, S.P. Tewari, G. Vaitheeswaran, J. Solid State Chem. 184 (2011) 343.